

Continuous-Wave Cavity Ring-Down for High-Sensitivity Polarimetry and Magnetometry Measurements

Dang-Bao-An Tran,^{1,2} Evan Edwards,¹ David P Tew,¹ Robert Peverall,¹ and Grant A D Ritchie^{1, a)}

¹⁾*Department of Chemistry, Physical and Theoretical Chemistry Laboratory, University of Oxford, South Parks Road, Oxford, OX1 3QZ, United Kingdom*

²⁾*Current Address: Time and Frequency Department, National Physical Laboratory, Teddington, TW11 0LW, United Kingdom*

We report the development of a novel variant of cavity ring-down polarimetry using a continuous-wave laser operating at 532 nm for highly precise chiroptical activity and magnetometry measurements. The key methodology of the apparatus relies upon the external modulation of the laser frequency at the frequency splitting between non-degenerate left- and right-circularly polarised cavity modes. The method is demonstrated by evaluation of the Verdet constants of crystalline CeF_3 and fused silica, in addition to the observation of gas- and solution-phase optical rotations of selected chiral molecules. Specifically, optical rotations of (i) vapours of α -pinene and R-(+)-limonene, (ii) mutarotating D-glucose in water, and (iii) acidified L-histidine solutions, are determined. The detection sensitivities for the gas- and solution-phase chiral activity measurements are $\sim 30 \mu\text{deg}$ and $\sim 120 \mu\text{deg}$ over a 30 s detection period per cavity roundtrip pass, respectively. Furthermore, the measured optical rotations for R-(+)-limonene are compared with computations performed using the Turbomole quantum chemistry package. The experimentally observed optically rotatory dispersion of this cyclic monoterpene was thus rationalised via consideration of its room temperature conformer distribution as determined by the aforementioned single-point energy calculations.

I. INTRODUCTION

Optical polarimetry is a fundamental technique for studying magnetometry and chirality, and has its basis in the rotation of the polarisation plane of linearly polarised light when passing through a magneto-optic or chiral medium, respectively. Magneto-optic rotational activity plays a key role in technologically important areas such as the development of novel Faraday rotators, magnetometry, and controlling light polarisation^{1–4}, while chirality is of crucial importance across many areas of science, from fundamental physics and investigations of parity violation^{5,6}, to pharmacology and biochemistry⁷.

Standard laboratory polarimeters have a typical detection precision no better than a few $\text{mdeg Hz}^{-1/2}$ that is limited by birefringence, and are suitable only for liquid-phase observations. It is important to be able to make precise measurements of optical rotation for all phases of matter and thus there has been a continuous effort to develop novel, more sensitive, and precise polarimetric methods^{8–10}. Particularly attractive in this regard is cavity-based polarimetry, which allows the interaction path length between the light and the magneto-optic/chiral medium to be increased manyfold, thus enhancing the detection sensitivity; for example, cavity ring-down techniques using a high-finesse linear cavity offer a large interaction path length between the light beam and sample of the order of a few km, compared to the few tens of cm afforded by a single cell. However, linear cavities without intracavity optics cannot be employed for chirality observations because the optical rotation is dependent upon the propagation direction of the light beam, and so is suppressed when the linearly polarised light passes back and forth between

two cavity mirrors. Vaccaro *et al.* circumvented this problem by developing pulsed laser-based cavity ring-down polarimetry (CRDP) by inserting a pair of intracavity quarter-wave plates to amplify the chiroptical rotation by the number of cavity roundtrip passes—the stress-induced birefringence of the intracavity optics, however, is correspondingly increased^{11–13}. This apparatus was used successfully in studying the gas-phase optical rotation of chiral molecules, and utilised a pulsed ns laser source. More recently, Bougas *et al.* demonstrated a continuous-wave (cw) variant of CRDP at 408 nm within a linear cavity for which the laser frequency is locked to a cavity resonance. Note, however, that this technique only applies for the measurement of the non-resonant Faraday effect of gases and magneto-optic crystals¹⁴, where the Faraday rotation is independent of the light propagation direction.

Given the limitations associated with using linear cavity geometries, a variety of CRDP instruments based upon bow-tie cavities have recently been demonstrated using pulsed and cw lasers. The first pulsed laser CRDP methodology using a bow-tie cavity was demonstrated by Rakitzis and co-workers, and employs two counter-propagating linearly (and orthogonally) polarised beams^{15–18}. An intra-cavity magneto-optic crystal is inserted into one arm of the cavity to provide a large bias rotation angle—the intracavity anisotropies of opposite symmetry are suppressed by a signal reversing technique. The chiroptical rotation is then extracted from the ring-down decay signals of the two counter-propagating beams. These instruments have ring-down times, τ , between 0.5 and 1 μs , and have been used for magnetometry measurements and chirality detection across a range of environments, including open air, pressure-controlled vapours, and the liquid phase, with precision $\geq 80 \mu\text{deg}$ per cavity pass. Recently, our group has demonstrated an implementation of bow-tie cavity-enhanced polarimetry with a cw laser source at 730 nm^{19,20}. A key feature of the method is the controlled perturbation of the laser

^{a)} Author to whom correspondence should be addressed: grant.ritchie@chem.ox.ac.uk

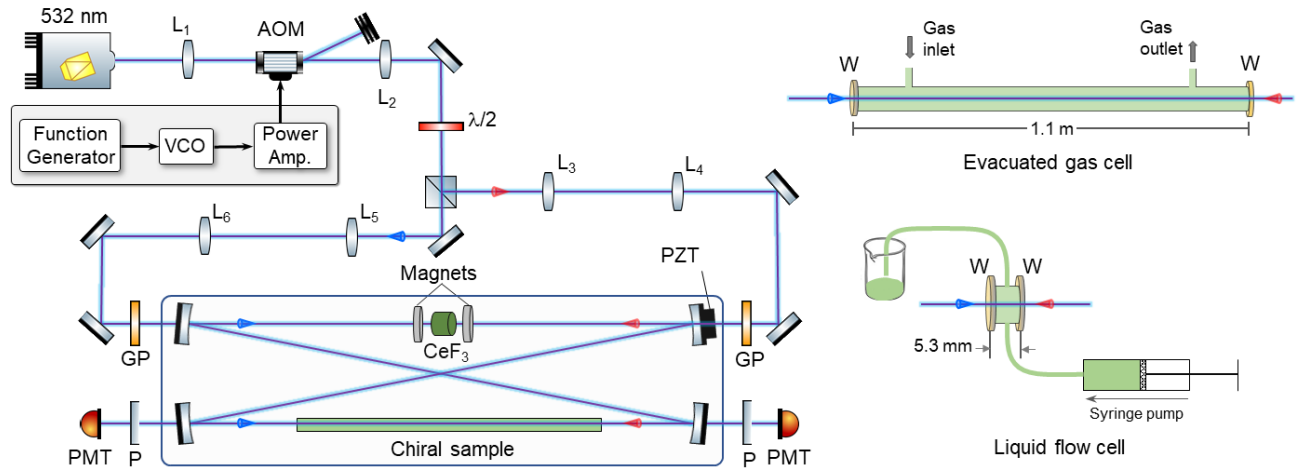


FIG. 1. Experimental setup for continuous-wave cavity ring-down polarimetry (CRDP) at 532 nm. Light from a diode-pumped solid-state (DPSS) laser at 532 nm is directed to an acousto-optic modulator (AOM). The first-order diffraction beam is separated into clockwise (CW) and counter-clockwise (CCW) beams and then mode matched with the TEM₀₀ mode of a bow-tie cavity comprising four high-reflectivity mirrors (M) ($R \geq 99.99\%$). A CeF₃ crystal is inserted into one arm of the cavity to provide a large bias rotation. For gas-phase optical rotation measurements of chiral samples, a 1.1 m long gas cell is inserted into the other arm of the cavity. For liquid-phase measurements, a 5 mm-long flow cell has been used. The CRD traces are detected by two photo-multiplier tubes (PMTs) and the polarisation states of these beams are analysed by two linear polarisers (P). VCO: voltage-controlled oscillator; GP: Glan-Taylor polariser; PZT: piezo-electric actuator; W: window; L: Lens

frequency, achieved by the addition of radiofrequency noise to its injection current, which leads to significant improvements in detection sensitivity. In addition, the use of cavity mirrors with a reflectivity $R \geq 99.99\%$, and low-loss intracavity optical components, enables τ values of $\sim 9 \mu\text{s}$. The detection precision was $\sim 10 \mu\text{deg}$ per cavity round trip for gas-phase optical rotation measurements. A means of achieving μdeg -level detection of optical rotation on the second timescale has recently been demonstrated using a frequency metrology method²¹; the chiroptical rotation is determined via the frequency splitting between the left- and right-circularly polarised cavity modes. Notably, this approach requires the laser frequency to be locked to the cavity resonance.

Most of the bow-tie cavity-based polarimeters mentioned above have employed intracavity Terbium Gallium Garnet (TGG) crystals to induce a large bias rotation or "offset" angle^{15–20}. However, TGG exhibits significant losses at wavelengths shorter than 600 nm, particularly in the spectral windows below 400 nm (due to the $\text{Tb}^{3+} {}^5\text{D}_3 \leftarrow {}^7\text{F}_6, {}^5\text{D}_2$ absorption bands) and around 490 nm (caused by the electronic transition ${}^5\text{D}_4 \leftarrow {}^7\text{F}_6$). These losses (significantly) limit the sensitivity of CRDP, and substitution for alternative magneto-optic materials is desirable. One such alternative, crystalline cerium fluoride (CeF₃) exhibits a lower absorption coefficient and a larger transparent spectral window (from 280 nm to 2500 nm) than TGG^{22,23}, making it one of the best candidates for developing highly sensitive CRDP in the UV, visible, and near-infrared regions. Indeed, recent work by Xygkis *et al.*²⁴ has identified CeF₃ as a Faraday-rotating crystal of high "figure of merit" for application in cavity ring-down polarimetry (on condition that the sample exhibits "ideal polishing").

In this paper, we first present the experimental setup for

our present implementation of CRDP using a *cw* laser operating at a fixed wavelength of 532 nm and show that external frequency modulation of the laser output at the frequency splitting between the left- and right-circularly polarised cavity modes leads to an increased detection sensitivity. We then demonstrate the high-precision measurement of the Verdet constant of crystalline CeF₃ and then present the gas-phase optical rotation measurement of enantiomers of α -pinene and R-(+)-limonene. These highly precise measurements are compared with state-of-the-art computations employing the Turbomole quantum chemistry package which elucidate the optical rotatory dispersion (ORD) curves exhibited by a relevant selection of individual limonene conformers. The paper concludes with two examples of liquid-phase CRDP. Firstly, the kinetics of D-glucose mutarotation are quantified. Subsequently, the variation of the optical rotation of L-histidine with decreasing pH is presented. The latter data are interpreted with a simple thermodynamic model which allows the optical rotation of the parent zwitterion, cation and dication to be estimated, these observations showcasing the particular utility of the apparatus for studies of aqueous solutions, and the characterisation of charge states that otherwise evade measurement.

II. HIGH-PRECISION MAGNETOMETRY WITH CW-CRDP

A. *cw*-CRDP Apparatus

Fig. 1 shows the experimental setup for CRDP at 532 nm. The operating principles of the cavity-enhanced

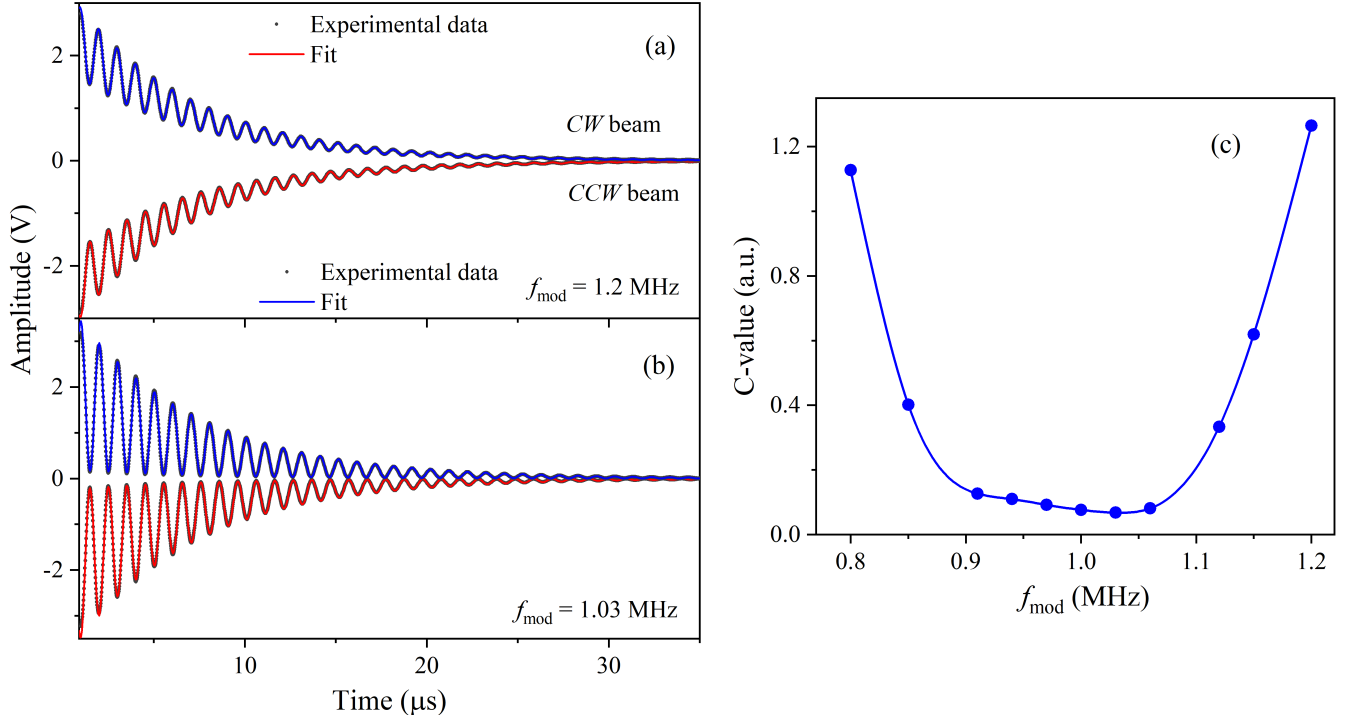


FIG. 2. (a–b) Cavity ring-down signals (dark points) from the CW and CCW beams for two different modulation frequencies applied to the laser light, $f_{\text{mod}} = 1.2$ and 1.03 MHz . The red and blue solid curves are the fits of the amplitude modulation model, as given by Eq. 1, to the data. The ring-down time is $\sim 6.5 \mu\text{s}$. (c) Variation of the polarisation-modulation depth as a function of f_{mod} . Experimental parameters: magnetic field of $\sim 0.15 \text{ T}$ giving ϕ_F of $\sim 3.2^\circ$; 2000 events averaged over 30 seconds.

continuous-wave polarimeter are explained in detail in previous publications^{19,20}, and here we only highlight the necessary differences between the laser sources and the optical setups.

A bow-tie cavity is constructed with four high-reflectivity plano-concave mirrors (Layertec, diameter of 12.7 mm). Each mirror has a reflectivity $R \geq 99.99\%$ at 532 nm . The total cavity length is $L = 557.8 \pm 0.4 \text{ cm}$ (width and length separations of $\sim 15 \text{ cm}$ and $\sim 139 \text{ cm}$, respectively). For scanning the cavity length, one of the cavity mirrors is mounted on a piezoelectric actuator (PZT, Piezomechanik GmBH) driven by a K-cube high-voltage piezo controller (Thorlabs, KPZ101). The polarimeter was addressed by a diode-pumped solid state (DPSS) laser at 532 nm (Verdi V5, Coherent) with a maximum power of 5 W . Typically, a laser power of $\sim 200 \text{ mW}$ was used. The laser beam is directed to an acousto-optic modulator (AOM, AA Opto-Electronic, MT80B30-A1.5-VIS) operated at a frequency of 80 MHz and which has a maximum fall time of $\sim 200 \text{ ns}$. The AOM is driven by a radiofrequency (rf) signal generated by a voltage-controlled oscillator (VCO, AA Opto-Electronic, DRFA10Y-B-0-50.110) with a tuneable frequency range between 65 and 95 MHz , and then power-booster by an rf power amplifier (AA Opto-Electronic, AMPB-B-30-10.500) with a gain of $\sim 34 \text{ dB}$. The AOM's driving frequency can be adjusted by a voltage signal provided by a function generator (Keysight, 33509B). The VCO is also controlled by a home-made TTL trigger box which acts as the master trigger to generate cavity ring-down signals fol-

lowing intracavity power build-up. The resulting first-order diffraction beam from the AOM has a power of $\sim 10 \text{ mW}$ and is directed to the cavity. A half-waveplate ($\lambda/2$, B-Halle) and a polarising beam-splitting cube (Thorlabs, PBS251) are used in tandem to separate the laser beam into two linearly polarised beams, p- and s-beams of clockwise (CW) and counter-clockwise (CCW) propagation, respectively. These beams are then injected into the cavity where they continue to propagate in opposing directions. Two Glan-Taylor polarisers (Thorlabs, GT10-A, extinction ratio $\geq 10^5$) are placed at the inputs of the cavity to filter and fix the polarisation states of the incident beams. A set of lenses is used to match the Gaussian spatial profile of the CW and CCW beams with the TEM_{00} mode of the cavity.

A *c*-oriented CeF_3 crystal (E-crystal Ltd., Japan) with a diameter of 12.7 mm and a thickness, l , of 2 mm is inserted into one arm of the cavity to induce a large offset rotation angle, ϕ_F . The crystal has been anti-reflection coated on both sides with a minimum reflectivity per surface of $\sim 0.15\%$ and has a Verdet constant, V , of $\sim 188 \text{ rad T}^{-1} \text{ m}^{-1}$ at 532 nm ^{22,23,26}. This crystal is located within a magnetic field of $B < 0.2 \text{ T}$, provided by a pair of ring neodymium magnets (First4Magnets), and produces a large Faraday offset angle of $\phi_F = VBl < 4^\circ$. Two linear polarisers (Thorlabs, LPVISC050-MP2, extinction ratio $\geq 10^5$) are placed at the outputs of the cavity to analyse the polarisation states of the output beams. The ring-down traces are measured by applying a triangular-wave signal with a frequency of $\sim 30 \text{ Hz}$ to

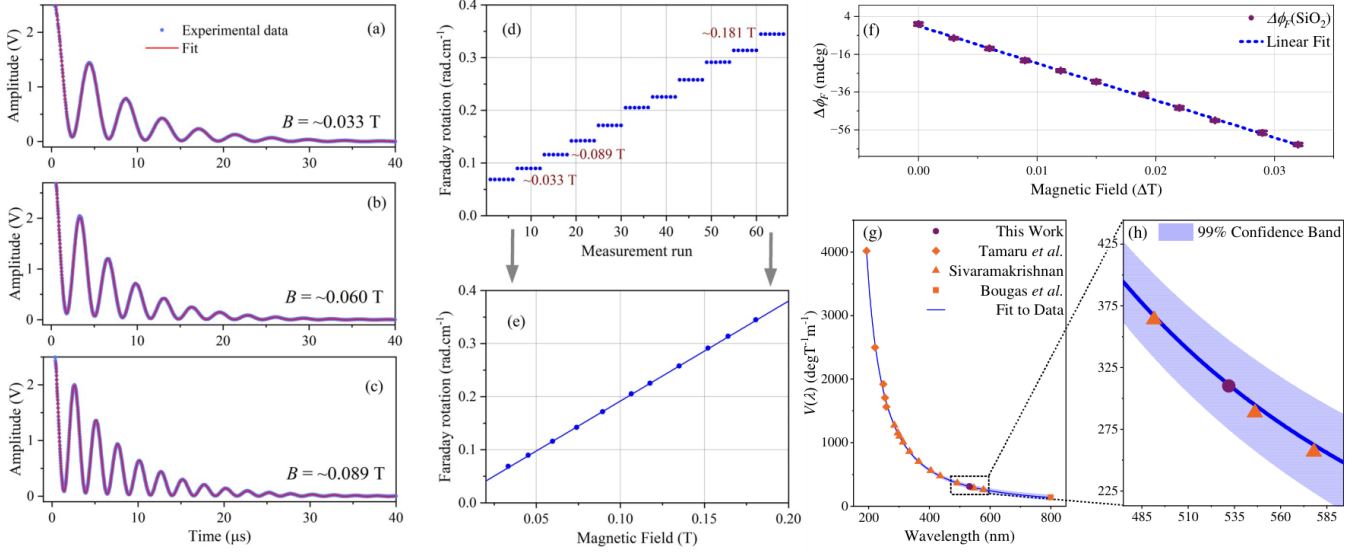


FIG. 3. The Faraday effect in crystalline CeF_3 and fused silica. (a–c) Cavity ring-down signal (dark points) at magnetic fields of 0.033, 0.060, and 0.089 T. For each recorded signal, ~ 2000 ring-down traces are averaged in 30 s. The red solid curves are fits of the amplitude modulation model, Eq. 1, to the data. (d–e) Variation of the Faraday rotation angle as a function of magnetic field. For each B field, six measurements are carried out (panel d, blue points) and the corresponding mean value is shown in panel e, (blue points). The blue line (panel e) is a linear fit to the data. (f–h) Faraday rotation measurements of a fused silica window and the corresponding Verdet dispersion calculation as compared with previous literature values from Tamaru *et al.*¹, Sivaramakrishnan²⁵, and Bougas *et al.*¹⁸.

the PZT driver and scanning the cavity length. The amplitude over which the cavity length is dithered is large enough to ensure that several cavity resonances are excited by the laser. As shown in Fig. 1, the ring-down signals are detected by two photo-multiplier tubes (Hamamatsu, R928) which are driven by two high-voltage power supplies (Stanford Research, SRS PS310). The signals are then amplified by two transimpedance amplifiers (Thorlabs, TIA 60) with a bandwidth of 60 MHz, and acquired by a 12-bit high resolution oscilloscope (Lecroy, WaveSurfer 4104HD, bandwidth of 1 GHz, 5 Gs/s sampling rate) that allowed the data to be averaged (typically 2000 events over 30 s). The detected signal is described by an exponential ring-down signal superimposed with a periodic function,

$$I(t) = I_0 e^{-t/\tau_0} [\cos^2(2\pi f t + \phi) + C], \quad (1)$$

in which I_0 is the maximum amplitude of the signal, τ_0 is the ring-down time, $f = c\phi/2\pi L$ is the polarisation beating frequency, with ϕ (rad) the single-pass rotation angle, ϕ the global phase offset, and C accounting for any reduction in the polarisation-modulation depth. The cavity ring-down time is ~ 6.5 μs, mainly limited by the optical losses on the CeF_3 crystal resulting from both reflections and optical absorption.

B. Improving the Sensitivity of the Polarimeter

Due to the Faraday effect²⁷, each cavity resonance is split into two circularly polarised modes, known as left- and right-resonant modes with a frequency separation of $\Delta f =$

$c\phi_F/\pi L$ (~ 1 MHz for $\phi_F = 3.2^\circ$). This separation is comparable with the bandwidth of the laser, and so the ring-down signal may be dominated by only one of these resonances, leading to a reduction in the modulation depth and thus limiting the detection sensitivity. In our recent works, we have perturbed the laser frequency by applying a Gaussian noise signal to the diode laser current, thus allowing the detection sensitivity to be improved by an order of magnitude^{19,20}. For the current setup using a fixed-frequency DPSS laser, perturbation of the laser frequency can be achieved via the driving frequency of the AOM. However, the slow rise time of the AOM (*ca.* 200 ns) makes this method inefficient, and therefore we choose as an alternative, to modulate the laser frequency via the AOM at the frequency splitting between the left- and right-circularly polarised modes, Δf . This perturbs both modes equally, promoting equal, simultaneous mode excitation, and so increases the observed polarisation-modulation depth thus enhancing the CRDP detection sensitivity.

To study the effect of this frequency modulation of the AOM's driving frequency on the polarisation-modulation depth, we have fixed the B field applied to the CeF_3 crystal at ~ 0.15 T (corresponding to $\Delta f \sim 1$ MHz), and recorded ring-downs over a range of modulation frequencies from 0.8 to 1.3 MHz. Fig. 2 (a–b) show exemplar ring-down signals (dark points) from the CW and CCW beams, recorded at modulation frequencies $f_{\text{mod}} = 1.2$ and 1.03 MHz, respectively. The red and blue solid curves are fits of the model given by Eq. 1 to the data. Fig. 2 (c) shows the variation of the polarisation-modulation depth as a function of f_{mod} . C approaches zero when the modulating frequency approximately equals the cavity mode splitting, Δf , from 0.95 to 1.07 MHz,

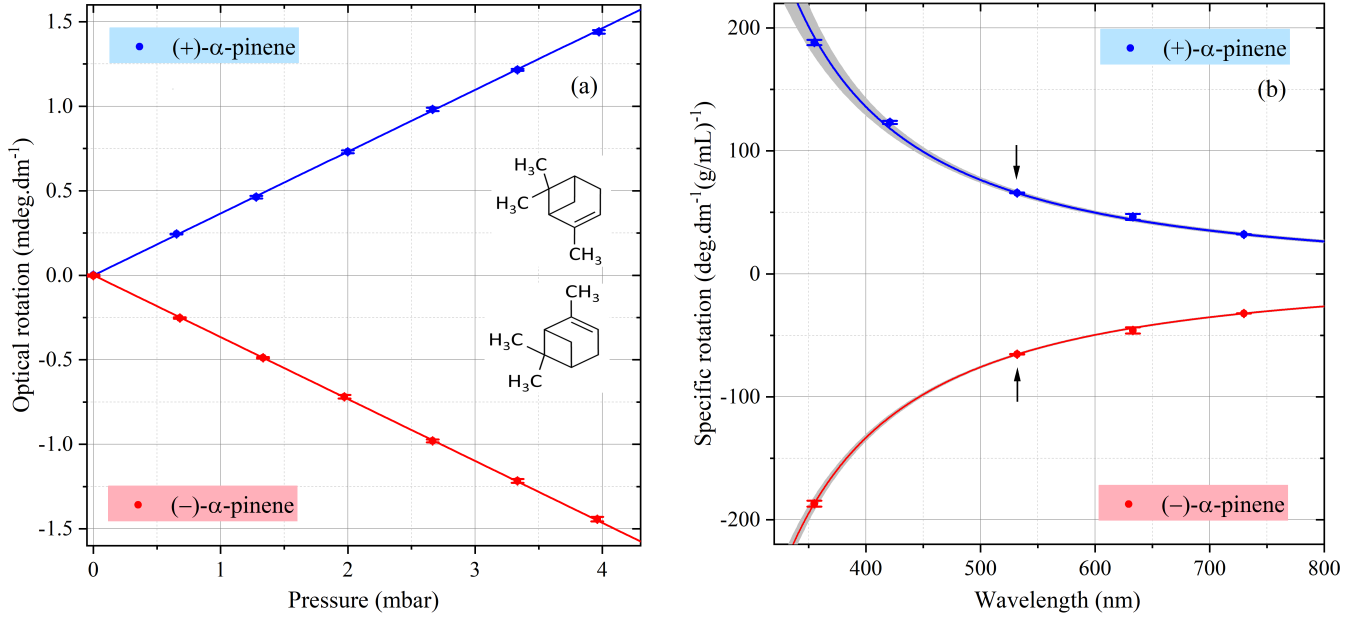


FIG. 4. Variation in optical rotation of enantiomers of α -pinene vapour as a function of pressure. Each data point and its error bar are given by the mean and standard deviation of the 10 measurements at a given pressure, respectively. The red and blue lines are weighted linear fits to the data. Experimental parameters: B field ~ 0.15 T (ϕ_F of $\sim 3.2^\circ$); 2000 events averaged over 30 s. (b) Variation of the specific rotation of (+)- and (-)- α -pinene as a function of wavelength (blue and red points, respectively). The black arrows indicate the optical rotation reported in this work. The grey solid curves are the fits of the wavelength dependence of the optical rotation to the data (see text for details), the grey areas representing the resulting mean prediction bands corresponding to a confidence level of 0.95.

allowing the detection sensitivity to be improved by around 1 order of magnitude²⁰.

C. Measurement of the Faraday Effect in CeF₃

With a Verdet constant similar in magnitude to that for TGG, CeF₃ has been identified as a suitable Faraday rotator for the UV and visible regions^{22–24,26}. In Fig. 3 we present measurements of the Faraday effect for crystalline CeF₃ at 532 nm. For these studies, only the CW beam is used, and its polarisation direction is rotated by a Faraday rotation angle ϕ_F . The magnetic field is varied between 0.03 and 0.18 T by changing the distance between the two ring magnets, and is precisely measured using a factory-calibrated Hall probe magnetometer (Hirst Magnetic Instruments, GM08) with a relative accuracy of $\sim 0.5\%$. For each B field, the modulation frequency f_{mod} has been chosen to be close to the cavity mode frequency splitting, allowing C to approach zero. This was achieved via manual variation of f_{mod} until maximum modulation depth had been attained. The Faraday rotation angle, $\phi_F = 2\pi Lf/c$, with c the speed of light, is determined by fitting Eq. 1 to the data.

Fig. 3 (a–c) show sample ring-down signals (blue points) and the corresponding fits to the data (solid red curves) at fields of $B = 0.033$, 0.060 , and 0.089 T. Fig. 3 (d) shows the Faraday rotation angle as the magnetic field ranges from 0.03 to 0.18 T. For each B field, six measurements were carried out and their mean values are shown in Fig. 3 (e) (blue

points), along with a linear fit to the data. The Verdet constant of CeF₃ is determined to be 188.4 ± 0.4 rad T⁻¹ m⁻¹ and is consistent with the value of ~ 188 rad T⁻¹ m⁻¹ derived from the Verdet constant dispersion model previously measured using a UV-IR spectrometer²¹, although marginally larger than the value of 171 rad T⁻¹ m⁻¹ obtained via an alternative linear, two-mirror cavity ring-down setup²⁴.

D. Evaluation of the Verdet Constant of Fused Silica

Fused silica represents another dielectric medium capable of exhibiting Faraday rotation. The material's broadband transparency and ubiquity in optical elements has motivated the characterisation of its magnetically induced circular birefringence. In a manner analogous to the aforementioned study, a cavity ring-down magnetometry analysis was conducted on a 6.35 mm-thick fused silica window measuring 1 inch in diameter and possessing ion beam sputtered anti-reflection coatings of 0.035% maximum reflectivity (Edmund Optics). In this instance, an electromagnet comprising a U-core (LEYBOLD® 562 11), a pair of coils (LEYBOLD® 562 13), and a brace of bored poles (LEYBOLD® 560 31), received current over a range of 1 Ampere (R&S® NGL202), the resulting magnetic field being estimated using a transverse Hall probe (GM08 Gaussmeter, Hirst Magnetic Instruments Ltd.). Ring-down traces were recorded at intervals of 0.1 A—the corresponding Faraday rotation measurements are displayed in figure 3 (f).

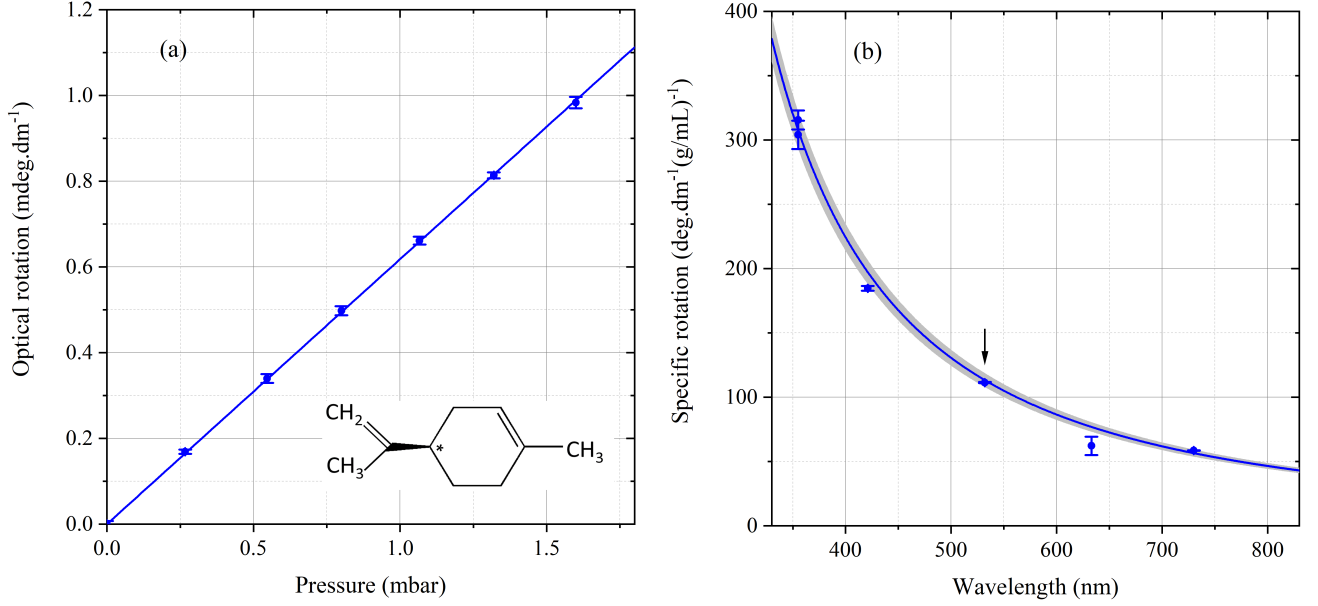


FIG. 5. (a) Gas-phase optical rotation measurements of R-(+)-limonene vapour over a range of pressures. Each data point and its error bar are given by the mean and the 2σ standard error of 10 measurements at a given pressure, respectively. The blue line is a weighted linear fit to the data. Experimental parameters: a magnetic field of ~ 0.15 T giving a ϕ_F of $\sim 3.2^\circ$; 2000 events averaged over 30 s. (b) Variation of the specific rotation of R-(+)-limonene as a function of wavelength (blue and red points, respectively). The black arrows indicate the optical rotation of enantiomers of R-(+)-limonene at 532 nm measured by our *cw*-CRDP apparatus. The grey solid curve is a fit of the wavelength dependence of the optical rotation to the data (see text for details), and the grey area is the mean prediction band resulting from the fits with a confidence level of 0.95.

A linear fit to the Faraday rotation measurements reveals a Verdet constant of $310 \pm 3 \text{ deg T}^{-1} \text{ m}^{-1}$ at 532 nm, in near-perfect agreement with interpolations of literature values^{1,18,25} recorded over a series of wavelengths (figures 3 (g) and (h)). The wavelength dependence of the Verdet constant depicted in these figures was modelled using the following functional form^{28–30}:

$$V(\lambda) = \frac{\alpha}{\lambda^2 - \lambda_0^2} + \beta \quad (2)$$

A fit of equation 2 to the data displayed in figure 3 (g) returned evaluated parameter values of $(8.045 \pm 0.207) \times 10^7 \text{ nm}^2 \text{ deg T}^{-1} \text{ m}^{-1}$, $8.464 \pm 18.020 \text{ deg T}^{-1} \text{ m}^{-1}$, and $130.9 \pm 2.0 \text{ nm}$ for α , β , and λ_0 , respectively.

III. GAS-PHASE MEASUREMENTS

The experimental apparatus described in section II has been used to perform measurements of gas-phase optical activity. If a chiral sample is introduced into one arm of the cavity, producing a chiroptical rotation, ϕ_C , then after each cavity roundtrip the polarisation states of the CW and CCW beams are rotated by an amount $\phi_{CW} = \phi_F + \phi_C$ and $\phi_{CCW} = \phi_F - \phi_C$, respectively. By fitting the ring-down traces to Eq. 1, the oscillating frequencies, $f_{CW} = c(\phi_F + \phi_C)/2\pi L$ and $f_{CCW} = c(\phi_F - \phi_C)/2\pi L$ can be determined, and thus the chiroptical

rotation is found to be

$$\phi_C = \frac{\pi L}{c} (f_{CW} - f_{CCW}). \quad (3)$$

To measure the optical rotation of gas phase chiral molecules, a 1.1 m-long gas cell was inserted into one arm of the cavity. The cell was enclosed by two 1 inch diameter, 6.35 mm thick fused silica windows (Edmund Optics, ion beam sputtered AR coated with $R < 0.035\%$). Each window was placed in a home-made mount and rested on two O-rings to minimise forces acting on the window, thus reducing birefringence. The gas pressure in the cell was measured by a capacitance pressure gauge (Leybold, CTR100, pressure range of 100 Torr). The cell was evacuated below 10^{-6} mbar using a compact turbo-molecular pump station (Pfeiffer, HiCube 300). Chiral samples were contained in a reservoir and their vapour injected into the gas cell via a dosing valve. A B field of ~ 0.15 T was applied to the CeF_3 crystal, corresponding to a Faraday rotation angle of $\phi_F \sim 3.2^\circ$. The empty cavity ring-down times for both beams are $\sim 4.7 \mu\text{s}$, corresponding to ~ 255 round trips and an effective path length through the gas cell of $\sim 280 \text{ m}$.

A. Gas-Phase Optical Rotation of (+)- and (–)- α -Pinene

Fig. 4 (a) shows the gas-phase optical rotation per unit length produced by the enantiomers of α -pinene (Sigma-

TABLE I. Reported values of the specific rotation of enantiomers of α -pinene and R-(+)-limonene in the gas phase. The final row presents the thermal average values at 295 K for R-(+)-limonene, determined from *ab-initio* calculations (see section III B).

Optically active sample	Assay purity	Optical purity (<i>ee</i>)	Optical rotation (deg dm ⁻¹ (g/ml) ⁻¹)				
			355 nm ¹¹	421 nm ²¹	532 nm	633 nm ¹²	730 nm ^{19,20}
(+)- α -pinene	99%	97%	188.2 \pm 2.2	123.2 \pm 1.3	65.81 \pm 0.30	46.3 \pm 2.5	32.10 \pm 0.13
(-)- α -pinene	99%	97%	-187.0 \pm 2.4		-65.90 \pm 0.20	-46.0 \pm 2.5	-32.21 \pm 0.11
R-(+)-limonene	97%	98%	315.5 \pm 7.4	184.6 \pm 1.8	110.49 \pm 0.47	62.1 \pm 7.1	59.83 \pm 0.25
			304.2 \pm 11				
R-(+)-limonene [†]	—	—	370.8	239.6 [‡]	139.3	94.9	69.8

[†]Calculation at 295 K

[‡]Interpolated value at 421 nm from data in Figure 6

Aldrich, enantiomeric excess *ee* = 97%) in the pressure range 0–4 mbar. Due to a combination of scattering and absorption of the intracavity light by α -pinene, the ring-down time decreases from 4.7 μ s to 4.2 μ s as the pressure increases from 0 to 4 mbar. Ten measurements were carried out at each pressure with f_{CW} and f_{CCW} determined by fitting data to Eq. 1, and ϕ_C then determined using Eq. 3. The uncertainty in ϕ_C for each measurement is calculated from the fitting errors of f_{CW} and f_{CCW} . There is a slight difference between f_{CW} and f_{CCW} even without the present of a chiral sample. This effect is due to the small inhomogeneities in the magnetic field and the slightly different propagation of the CW and CCW beams through the CeF₃ crystal, and potentially in addition to the presence of non-planarity-induced optical rotation (NPI-OR), a phenomenon described and quantified in work by Bougas and co-workers¹⁸. We therefore introduce a frequency offset $\delta = f_{CW} - f_{CCW}$ to Eq. 3; δ is \sim 1 kHz and does not change during a set of measurements. Values for ϕ_C and its errors are the weighted mean and 2 σ weighted standard error of the ten measurements at each pressure respectively. The optical rotation precision is \sim 30 μ deg per cavity pass over a 30 s detection period, as given by the error bar for ϕ_C . This corresponds to a time-averaged sensitivity of \sim 164 μ deg Hz^{-1/2}, and is \sim 3 times better than compared to previous pulsed CRDP investigations at 532 nm¹⁶ but less than that of the *cw*-CRDP approach reported at 730 nm²⁰ (\sim 10 μ deg per cavity pass). This is due to the larger optical losses incurred by use of an intra-cavity CeF₃ crystal in the present setup. The red and blue solid lines are linear weighted fits to the data and possess gradients $d\phi_C/dp = 0.3655 \pm 0.0015$ mdeg dm⁻¹ mbar⁻¹ for (+)- α -pinene, and -0.3660 ± 0.0009 mdeg dm⁻¹ mbar⁻¹ for (-)- α -pinene. The gas-phase specific optical rotation, $[\alpha]_{532 \text{ nm}}^{295 \text{ K}}$, is thus determined to be 65.81 ± 0.30 deg dm⁻¹ (g/ml)⁻¹ for (+)- α -pinene and -65.45 ± 0.20 deg dm⁻¹ (g/ml)⁻¹ for (-)- α -pinene at a wavelength of 532 nm and a temperature of 22°C, where the quoted uncertainty includes a contribution related to the lengths of the intracavity gas cell and the cavity itself, the magnitude of which corresponds to \sim

0.11 deg dm⁻¹ (g/ml)⁻¹.

To our knowledge, these are the first measurements of the gas-phase optical rotations of enantiomers of α -pinene at 532 nm. Previously, similar gas-phase optical rotation measurements on α -pinene (*ee* \sim 97%) enantiomers have been demonstrated at 355 nm and 633 nm by Vaccaro *et al.* at 25°C^{11,12}, and at 730 nm by our group at 22°C^{19,20}. The rotation of nominally enantiomerically pure (+)- α -pinene at 421 nm and 21°C²¹ has also recently been reported. These measurements are summarised in Table I. It is noted that the gas-phase optical rotation of (+)- and (-)- α -pinene at 800 nm has also been reported by Sofikitis *et al.*, with reported rotations of 17.57 ± 0.57 and -18.04 ± 0.98 deg dm⁻¹ (g/ml)⁻¹, respectively. The enantiomeric excess of the samples has not, however, been provided¹⁵.

Fig. 4 (b) shows the measured rotatory powers of the two α -pinene enantiomers between 355 and 730 nm. Assuming that the optical rotation is dominated by the intense $\pi \rightarrow \pi^*$ transition at around 200 nm, the ORD curve can be modelled as

$$[\alpha]_{\lambda}^T = \frac{A_T}{(\lambda^2 - \lambda_0^2)} \quad (4)$$

where A_T is the temperature-dependent amplitude and λ_0 is the resonant wavelength of the electronic transition that produces the chiroptical rotation³⁰. The blue and red solid curves are weighted fits of this simple model to the data. Fig. 4 (b) also shows the mean prediction band resulting from the fits with a confidence level of 0.95 (grey areas). The resulting closest UV transition and the optical rotation amplitude are found to be $\lambda_0 = 205 \pm 2$ nm (210 ± 2 nm when including the reported measurement at 421 nm) and $A_T = (1.575 \pm 0.006) \times 10^7$ ($(1.571 \pm 0.019) \times 10^7$ including measurement at 421 nm) deg dm⁻¹ (g/mL)⁻¹ nm² for (+)- α -pinene, and $\lambda_0 = 203 \pm 2$ nm and $A_T = (1.583 \pm 0.005) \times 10^7$ deg dm⁻¹ (g/mL)⁻¹ nm² for (-)- α -pinene.

B. Gas-Phase Optical Rotation of R-(+)-Limonene

The gas-phase chiroptical power of R-(+)-limonene (Sigma-Aldrich, $ee = 99\%$) has also been quantified and Fig. 5 (a) shows its optical rotation per unit length as a function of pressure between 0 and 1.6 mbar. Due to a combination of optical absorption and scattering, τ is observed to decrease from 4.7 μs for zero sample pressure to $\sim 2.5 \mu\text{s}$ at 1.6 mbar; the error bar for each data point correspondingly increasing with pressure. The linear weighted fit to the data has gradient $d\phi_C/dp = (0.6147 \pm 0.0024) \text{ mdeg dm}^{-1} \text{ mbar}^{-1}$ from which the optical rotation is determined to be $(110.49 \pm 0.47) \text{ deg dm}^{-1} (\text{g/mL})^{-1}$ at 532 nm and 22°C. The quoted uncertainty of the specific rotation includes a systematic uncertainty relating to the intracavity gas-cell and cavity lengths. There is, to our knowledge, only one other gas-phase optical rotation measurement of R-(+)-limonene (assay $\geq 95\%$, unknown enantiomeric excess) at 532 nm¹⁶ with a reported specific rotation of $\sim 70 \text{ deg dm}^{-1} (\text{g/mL})^{-1}$. Measurements of the optical rotation of R-(+)-limonene vapour have been performed at 355 and 633 nm at 25°C^{11,12}, at 421 nm at 21°C²¹, and 730 nm at 22°C²⁰. The findings of these studies are summarised in Table I and displayed in Fig. 5 (b). Noting that there are also weak transitions at 174.5, 210, 218 and *ca.* 400 nm in limonene^{31,32}, if we assume that the optical rotation is dominated by the intense $\pi \rightarrow \pi^*$ transition of the cyclohexane moiety at 186 nm, then the simple model given by Eq. 4 can be used to describe the ORD curve of R-(+)-limonene. The blue solid line in Fig. 5 (b) is then the weighted fit to the data for which the electronic transition is fixed at $\lambda_0 = 186 \text{ nm}$. Within this crude estimation, the resulting optical rotation amplitude is found to be $A_T \sim (2.81 \pm 0.05) \times 10^7 \text{ deg dm}^{-1} (\text{g/mL})^{-1} \text{ nm}^2$. Once again, the grey area encompassing the blue line represents a 95% confidence level.

Limonene is a cyclic monoterpene and at room temperature can exist in three distinct conformers (rotamers) defined by a relative moiety rotation about a single bond such that eclipsing interactions between the ring and isopropenyl moiety are minimised. The different conformers (denoted 1 to 3, with increasing enthalpy) are depicted as Newman projections in Fig. 6 (upper panes) and have relative energies 0, 0.44, and 1.91 kJ mol^{-1} , respectively. These energies were obtained from CCSD(T)(F12*)/aug-cc-pVQZ single point energy calculations^{33–36} at B3LYP/def2-TZVPP optimised geometries, accounting for vibrational zero-point energy at the B3LYP/def2-TZVPP level of theory.^{37–39} Including a correction for the zero-point energy yields relative energies of 0, 0.89 and 2.28 kJ mol^{-1} for the three conformers, which shifts the thermal average slightly, as shown in Fig. 6. ORD values for each conformer were computed using linear response⁴⁰ with the CAM-B3LYP functional⁴¹ in the length representation with the aug-cc-pVQZ basis set.³⁶ The calculations reveal that each of the conformers exhibit a different optical rotatory power, the interplay of which dictates the calculated (and experimentally observed) ORD curves shown in Fig. 6. Notably, two of the three conformers (1 and 3) display optical rotations that are smaller in magnitude and of the opposite sense

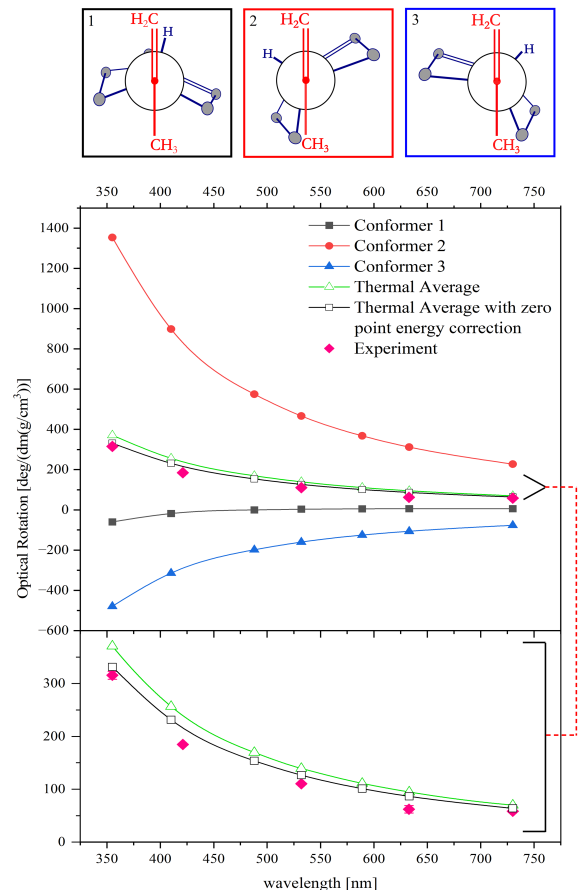


FIG. 6. Three distinct conformers of limonene depicted as Newman projections (upper panes) and associated *ab-initio* ORD curves (lower graph). The 295 K thermal averages (with and without zero-point energy corrections) are shown as well as the experimental results collated in Table I (pink diamonds). The lower pane is a zoom of the thermal averages and experimental results

to the other (2); at room temperature (295 K) the population-weighted rotation for conformer 2 dominates. The thermal average rotation is shown by the green unfilled triangles in Fig. 6 and is in reasonable agreement with experiment.

IV. LIQUID-PHASE MEASUREMENTS

For measuring the chiroptical properties of aqueous samples, a home-made 5.3 mm-long flow cell was inserted into one arm of the cavity (see Fig. 1). The cell consists of two fused silica windows (Layertec GmbH) which are AR coated for the air/fused-silica interface ($R < 0.1\%$) and non-coated for the water/fused-silica interface. These windows are separated by a FFKM O-ring (Polymax, thickness of $5.30 \pm 0.03 \text{ mm}$) and mounted on two kinematic cage-compatible mounts (Thorlabs, KC1/M). Chiral aqueous solutions were injected into the flow cell using a syringe pump (Harvard Appa-

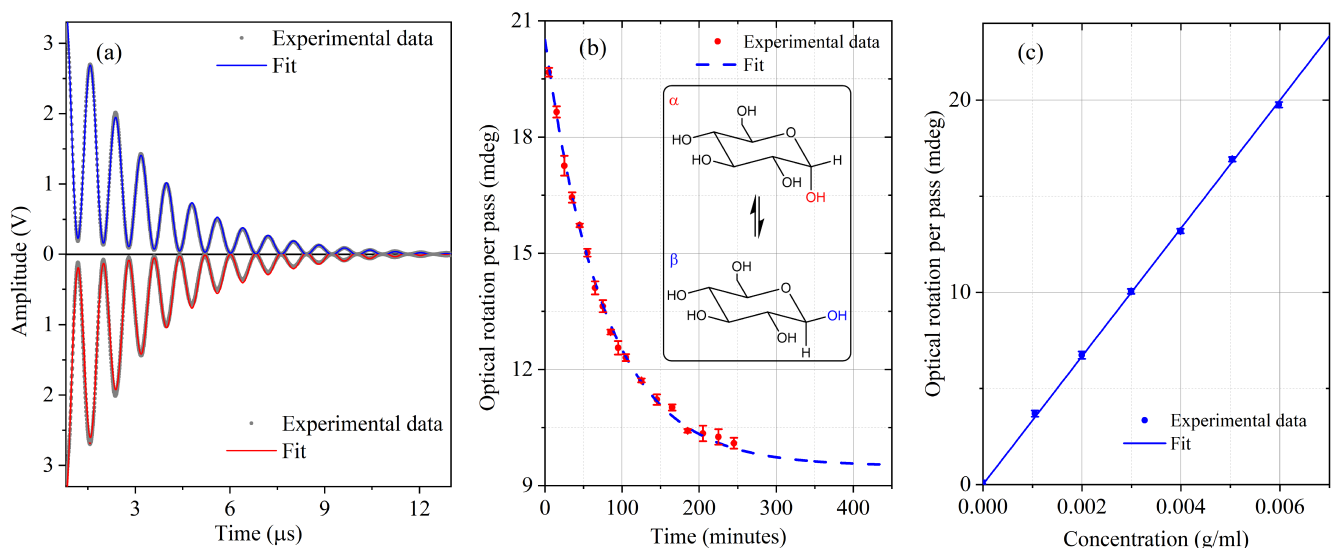


FIG. 7. Liquid-phase optical rotation measurements of chiral aqueous samples. (a) Cavity ring-down signals (dark points) from the CW and CCW beams probing liquid water. The red and blue solid curves are fits of Eq. 1 to the data. τ is $\sim 2.5 \mu\text{s}$. Experimental parameters: B field $\sim 0.15 \text{ T}$ ($\phi_F \sim 3.2^\circ$); 2000 events averaged over 30 s. (b) Variation of rotation angle per round-trip pass in the cavity for 0.003 g/mL D-glucose as a function of time (red points). Each data point and its error are the average and standard error of 5 data sets, respectively. The dashed blue curve is a weighted exponential fit to the data. (c) Variation of optical rotation angle per round-trip pass in the cavity as a function of D-glucose concentration (after 5 hours waiting time). Each data point and its error are the average and standard error of 10 data sets at the given concentration, respectively. The blue line is a weighted linear fit to the data.

ratus, 11) with a flow rate of $\sim 0.2 \text{ mL min}^{-1}$. Once again, a B field of $\sim 0.15 \text{ T}$ was applied to the CeF_3 crystal ($\phi_F \sim 3.2^\circ$). Fig. 7 (a) shows typical ring-down signals observed with the flow cell filled with water. Each signal is an average of 2000 events over 30 seconds. τ is $\sim 3 \mu\text{s}$ and corresponds to ~ 135 round trips in the cavity and an effective path length through the flow cell of $\sim 0.72 \text{ m}$.

A. Mutarotation of D-Glucose

We use this apparatus to probe the mutarotation of D-glucose via measurement of its specific rotation—where the dissolved chiral molecules eventually equilibrate between different anomers. Mutarotation manifests as a time dependent change in the specific rotation (as the two anomers in this case have different specific rotations), and Fig. 7 (b) shows the time evolution of the optical rotation angle for $3 \times 10^{-3} \text{ g/mL}$ D-glucose in water over a period of 250 minutes. For each time point, 5 measurements were carried out over a total observation duration of 75 s. Each data point and its error bar in Fig. 7 (b) are given by the weighted mean and the standard error of the five measured rotation angles, respectively. The reaction kinetics are well described by a simple, first-order exponential model $\phi_C(t) = \phi_{C, t \rightarrow \infty} + Ae^{-kt}$ (dashed curve). Fitting this to the data reveals a rate constant for mutarotation of $k = 1.298 \pm 0.047 \times 10^{-2} \text{ min}^{-1}$ at 18°C , in good agreement with recent broadband Mueller ellipsometry measurements conducted by Vala *et al.*⁴²

Fig. 7 (c) shows the specific rotation of D-glucose in water

as the mutarotation approaches completion (~ 5 hours observation period). Each data point and its error are the average and the standard error of 10 data sets at a given concentration, respectively. The optical rotation of D-glucose is determined to be $62.96 \pm 0.38 \text{ deg dm}^{-1} (\text{g/mL})^{-1}$ at 532 nm , where the quoted uncertainty of the specific rotation includes a systematic uncertainty relating to the intracavity gas cell and cavity lengths.

B. pH-Dependent Optical Rotation of L-Histidine

The apparatus has also been used to investigate the optical activity of chiral amino acids and the variation of the same as a function of the solution environment. As an example, we present data describing how the optical rotation of L-histidine varies as a function of both its own concentration as well as the solution acidity. The results are discussed in light of the well documented Clough-Lutz-Jirgensons (CLJ) rule⁴³. Finally, a thermodynamic analysis is conducted in order to ascertain the concentration profiles of the various ionic species in solution, from which the optical rotations of the latter can be approximated. The results of this calculation thus provide a quantitative interpretation of the observed CLJ behaviour.

The total optical rotation of L-histidine was measured as a function of amino acid concentration under three environments: 0.0, 0.1, and 0.2 M $\text{HCl}_{(\text{aq})}$. The results are shown in Fig. 8 (a). The CLJ rule, namely that the acidification of an aqueous solution of an L-amino acid causes a positive increase in its optical rotation⁴³, is clearly observed and is con-

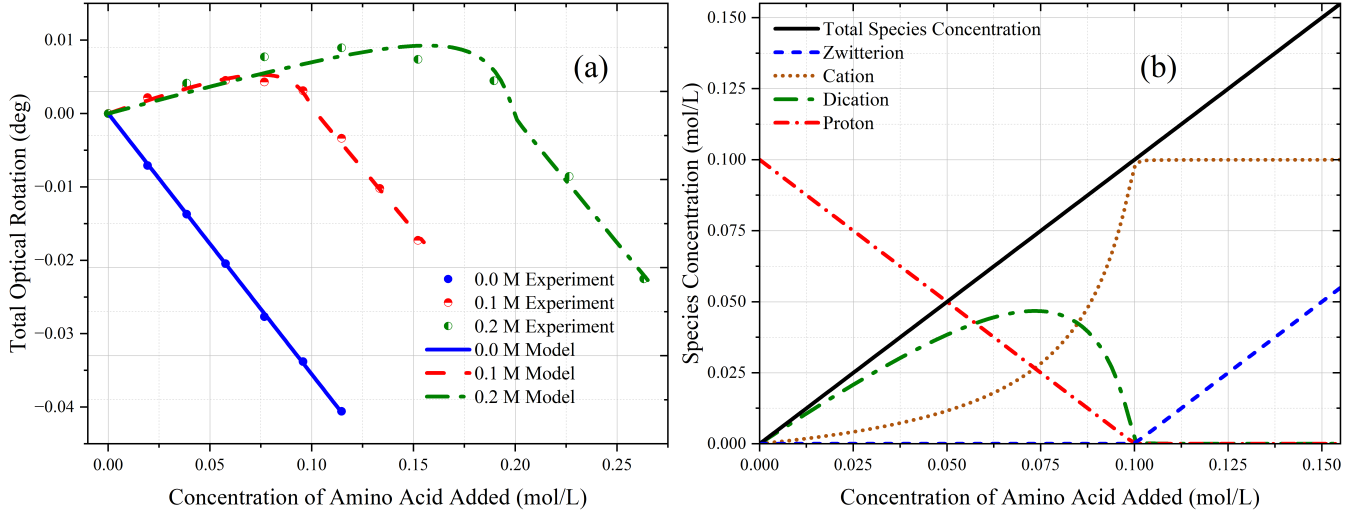


FIG. 8. pH-dependent optical rotation of L-histidine. (a) Experimental findings for optical rotation of L-histidine under three acidity regimes compared with modeled values (see text for details). (b) Representative calculated concentration profile for L-histidine charge states in solution, alongside the predicted "free proton" concentration, in the presence of 0.1 M $\text{HCl}_{(\text{aq})}$.

sistent with previous experimental findings⁴⁴. In order to interpret the data presented in Fig. 8 (a), concentration profiles of the chiral species in solution, each of which contributes to the observed rotation, were calculated. This was achieved by solving the below system of equations over the amino acid concentration range ($[\text{AA}_{\text{tot}}]$) for the three environments studied, in which $[\text{H}^+]$ denotes the concentration of "free protons", i.e., hydroxonium ions, in solution. It must be noted that this represents only a preliminary investigation, and neglects electrostatic contributions and previously-documented phenomena such as specific anion effects⁴⁵.

$$[\text{AAH}^+] K_{a_1} - [\text{AA}^\pm] [\text{H}^+] = 0 \quad (5)$$

$$[\text{AAH}_2^{2+}] K_{a_2} - [\text{AAH}^+] [\text{H}^+] = 0 \quad (6)$$

$$[\text{AAH}^+] + [\text{AAH}_2^{2+}] + [\text{H}^+] - [\text{HCl}] = 0 \quad (7)$$

$$[\text{AA}^\pm] + [\text{AAH}^+] + [\text{AAH}_2^{2+}] - [\text{AA}_{\text{tot}}] = 0 \quad (8)$$

Under the experimental conditions used, it can be assumed that only the zwitterion, cation and dication of L-histidine could be present in significant quantities in solution. In the above equalities, the concentrations of these species are represented as $[\text{AA}^\pm]$, $[\text{AAH}^+]$ and $[\text{AAH}_2^{2+}]$, respectively. Of these equations, 5 and 6 represent the acid dissociation equilibria of the cation and dication, respectively, where $\text{p}K_{a_1}$ (corresponding to the imidazole side chain of the histidine molecule) was taken to be 6.00 while $\text{p}K_{a_2}$ (representing the carboxylic acid moiety) was set equal to 1.82⁴⁶. Eq. 7 accounts for electroneutrality in the bulk solution, with 8 describing the system's mass balance. The results of one such set of concentration profile evaluations are depicted in Fig. 8 (b).

With the concentration profiles in hand, a sequential least squares programming (SLSQP) method, fitting to the experimental findings, was employed to determine the optimised

Optically active sample	Optical Rotation ($\text{deg dm}^2/\text{mol}$)		
	This work	Theory ^{a,b}	Experimental ⁴³
L-His [±]	-6.693	-6.24, -4.57	-5.98
L-His ⁺	0.095	-, -	-
L-His ²⁺	1.533	10.54, 8.83	1.83

TABLE II. Predicted optical rotation values for L-histidine species in solution. ^{a,b}Results of time-dependent density functional theory calculations using B3LYP (a) and BHLYP (b) functionals⁴⁷.

values for the individual optical rotations. This was conducted for all three environments simultaneously under the assumption that the optical rotation of an individual species does not change dramatically between each condition set. The results of these calculations are displayed in Table II. The total optical rotation is a concentration-weighted sum of the contributions from each species in solution, and so the optimised individual rotations can be used to infer the predicted total observed rotation as a function of amino acid concentration at each acidity regime. This analysis was conducted and the results are depicted in Fig. 8 (a).

It is noteworthy that this simple, first-principles methodology shows quite good agreement with both theoretical⁴⁷ and experimental⁴³ values, some of which are also displayed in Table II. For example, at 532 nm we predict an $8.23 \text{ deg dm}^2 \text{ mol}^{-1}$ rotation increase from zwitterion to dication, agreeing well with Greenstein's experimental finding of $7.81 \text{ deg dm}^2 \text{ mol}^{-1}$ at 589.3 nm. Notably, this analysis provides access to approximate optical rotations of intermediate charge states, in this case the monocation, otherwise difficult

to extract directly from experimental observations.

V. CONCLUSIONS

We have developed a new variant of continuous-wave CRD polarimetry using a fixed-wavelength laser source at 532 nm. The sensitivity of this apparatus is optimised via frequency modulation of the laser output to regularly and simultaneously excite both the non-degenerate left- and right-circularly polarised cavity modes. The CRDP technique has been demonstrated by evaluating the Verdet constants of CeF_3 and fused silica, as well as the gas-phase optical rotation of (+)- and (−)- α -pinene, and (R)-(+)-limonene. The limit of precision for the gas-phase optical rotation measurements is $\sim 30 \mu\text{deg}$ per cavity pass, limited by the optical losses on the CeF_3 crystal, and the uncertainty on the specific optical rotation is better than $0.3 \text{ deg dm}^{-1} (\text{g/mL})^{-1}$. The measurements of limonene are interpreted via state-of-the-art computational evaluations of the optical rotations of the three thermally accessible conformers of this species in the gas phase. Their relative energies were determined to span a range of approximately 2 kJ mol^{-1} . In addition, the CRDP technique has been extended to measurements in the liquid phase with a limit of detection of $\sim 120 \mu\text{deg}$ per cavity pass, corresponding to a time-averaged sensitivity of $\sim 657 \mu\text{deg Hz}^{-1/2}$. Specifically, the mutarotation of D-glucose has been tracked over 4 hours and a rate constant for mutarotation of $k = 1.298 \pm 0.047 \times 10^{-2} \text{ min}^{-1}$ at a temperature of 18°C was determined. Finally, the optical rotation of L-histidine has been determined as a function of the total amino acid concentration, and the acidity of the solution. These measurements allowed estimation of the optical rotatory powers of the aqueous L-histidine zwitterion, cation and dication, thus presenting a promising means of evaluating the chiroptical properties of otherwise unobservable charge states in solution. The results of these final investigations also provide accessible, empirical quantification of the time-tested Clough-Lutz-Jirgensons rule for amino acids.

ACKNOWLEDGMENTS

This work was funded by the European Commission Horizon 2020, ULTRACHIRAL Project (grant no. FETOPEN, ID no. 737071).

DATA AVAILABILITY

The data that support the findings of this study are available from the corresponding author upon reasonable request.

REFERENCES

- ¹Y. Tamaru, H. Chen, A. Fuchimukai, H. Uehara, T. Miura, and R. Yasuhara, “Wavelength dependence of the verdet constant in synthetic quartz glass for deep-ultraviolet light sources,” *Optical Materials Express* **11**, 814–820 (2021).
- ²H. Kato, T. Matsushita, A. Takayama, M. Egawa, K. Nishimura, and M. Inoue, “Theoretical analysis of optical and magneto-optical properties of one-dimensional magnetophotonic crystals,” *Journal of Applied Physics* **93**, 3906–3911 (2003).
- ³M. Inoue, K. Arai, T. Fujii, and M. Abe, “Magneto-optical properties of one-dimensional photonic crystals composed of magnetic and dielectric layers,” *Journal of applied physics* **83**, 6768–6770 (1998).
- ⁴N. Edwards, S. Phipp, P. Baird, and S. Nakayama, “Precise measurement of parity nonconserving optical rotation in atomic thallium,” *Physical review letters* **74**, 2654 (1995).
- ⁵A. Courmol, M. Manceau, M. Pierens, L. Lecordier, D. Tran, R. Santagata, B. Argence, A. Goncharov, O. Lopez, M. Abgrall, *et al.*, “A new experiment to test parity symmetry in cold chiral molecules using vibrational spectroscopy,” *Quantum Electronics* **49**, 288 (2019).
- ⁶B. Darquié, C. Stoeffler, A. Shelkovnikov, C. Daussy, A. Amy-Klein, C. Chardonnet, S. Zrig, L. Guy, J. Crassous, P. Soullard, *et al.*, “Progress toward the first observation of parity violation in chiral molecules by high-resolution laser spectroscopy,” *Chirality* **22**, 870–884 (2010).
- ⁷R. Corradini, S. Sforza, T. Tedeschi, and R. Marchelli, “Chirality as a tool in nucleic acid recognition: Principles and relevance in biotechnology and in medicinal chemistry,” *Chirality: The Pharmacological, Biological, and Chemical Consequences of Molecular Asymmetry* **19**, 269–294 (2007).
- ⁸P. L. Polavarapu, “Renaissance in chiroptical spectroscopic methods for molecular structure determination,” *The Chemical Record* **7**, 125–136 (2007).
- ⁹P. L. Polavarapu, “Determination of the absolute configurations of chiral drugs using chiroptical spectroscopy,” *Molecules* **21**, 1056 (2016).
- ¹⁰P. L. Polavarapu and E. Santoro, “Vibrational optical activity for structural characterization of natural products,” *Natural Product Reports* **37**, 1661–1699 (2020).
- ¹¹T. Müller, K. B. Wiberg, and P. H. Vaccaro, “Cavity ring-down polarimetry (crdp): a new scheme for probing circular birefringence and circular dichroism in the gas phase,” *The Journal of Physical Chemistry A* **104**, 5959–5968 (2000).
- ¹²S. M. Wilson, K. B. Wiberg, J. R. Cheeseman, M. J. Frisch, and P. H. Vaccaro, “Nonresonant optical activity of isolated organic molecules,” *The Journal of Physical Chemistry A* **109**, 11752–11764 (2005).
- ¹³C. L. Craft, P. M. Lemler, and P. H. Vaccaro, “Optical activity in saturated cyclic amines: Untangling the roles of nitrogen-inversion and ring-puckering dynamics,” *The Journal of Physical Chemistry A* **125**, 5562–5584 (2021).
- ¹⁴J. C. Visschers, O. Tretiak, D. Budker, and L. Bougas, “Continuous-wave cavity ring-down polarimetry,” *The Journal of Chemical Physics* **152**, 164202 (2020).
- ¹⁵D. Sofikitis, L. Bougas, G. E. Katsoprinakis, A. K. Spiliotis, B. Loppinet, and T. P. Rakitzis, “Evanescent-wave and ambient chiral sensing by signal-reversing cavity ringdown polarimetry,” *Nature* **514**, 76–79 (2014).
- ¹⁶A. Spiliotis, M. Xygkis, E. Klironomou, E. Kardamaki, G. Boulogiannis, G. Katsoprinakis, D. Sofikitis, and T. Rakitzis, “Gas-phase optical activity measurements using a compact cavity ringdown polarimeter,” *Laser Physics* **30**, 075602 (2020).
- ¹⁷A. Spiliotis, M. Xygkis, E. Klironomou, E. Kardamaki, G. Boulogiannis, G. Katsoprinakis, D. Sofikitis, and T. Rakitzis, “Optical activity of lysozyme in solution at 532 nm via signal-reversing cavity ring-down polarimetry,” *Chemical Physics Letters* **747**, 137345 (2020).
- ¹⁸L. Bougas, D. Sofikitis, G. E. Katsoprinakis, A. K. Spiliotis, P. Tzallas, B. Loppinet, and T. P. Rakitzis, “Chiral cavity ring down polarimetry: Chirality and magnetometry measurements using signal reversals,” *The Journal of Chemical Physics* **143** (2015), 10.1063/1.4930109, 104202, https://pubs.aip.org/aip/jcp/article-pdf/doi/10.1063/1.4930109/15503604/104202_1_online.pdf.
- ¹⁹D.-B.-A. Tran, K. M. Manfred, R. Peverall, and G. A. Ritchie, “Continuous-wave cavity-enhanced polarimetry for optical rotation measurement of chiral molecules,” *Analytical Chemistry* **93**, 5403–5411 (2021).
- ²⁰D.-B.-A. Tran, R. Peverall, S. Rosson, K. M. Manfred, G. A. Ritchie, *et al.*, “High performance continuous-wave laser cavity enhanced polarimetry using rf-induced linewidth broadening,” *Optics Express* **29**, 30114–30122

¹Y. Tamaru, H. Chen, A. Fuchimukai, H. Uehara, T. Miura, and R. Yasuhara, “Wavelength dependence of the verdet constant in synthetic quartz glass

- (2021).
- ²¹L. Bougas, J. Byron, D. Budker, and J. Williams, "Absolute optical chiral analysis using cavity-enhanced polarimetry," *Science Advances* **8**, eabm3749 (2022).
 - ²²V. Vasyliiev, E. G. Villora, M. Nakamura, Y. Sugahara, and K. Shimamura, "Uv-visible faraday rotators based on rare-earth fluoride single crystals: LIREF4 (RE = Tb, Dy, Ho, Er and Yb), PrF3 and CeF3," *Opt. Express* **20**, 14460–14470 (2012).
 - ²³P. Molina, V. Vasyliiev, E. Villora, and K. Shimamura, "Cef 3 and prf 3 as uv-visible faraday rotators," *Optics Express* **19**, 11786–11791 (2011).
 - ²⁴M. Xygkis, A. N. Linaraki, E. N. Toutoudaki, G. E. Katsoprinakis, and T. P. Rakitzis, "Absorption coefficients and scattering losses of TGG, TGP, KTF, FS, and CeF₃ magneto-optical crystals in the visible via cavity ring-down spectroscopy," *Appl. Opt.* **62**, 7730–7735 (2023).
 - ²⁵V. Sivaramakrishnan, "Dispersion of faraday rotation in fused quartz," *Proceedings of the Indian Academy of Sciences-Section A*, **44**, 206–215 (1956).
 - ²⁶E. G. Villora, K. Shimamura, and G. R. Plaza, "Ultraviolet-visible optical isolators based on cef3 faraday rotator," *Journal of Applied Physics* **117**, 233101 (2015).
 - ²⁷D. Budker, W. Gawlik, D. Kimball, S. Rochester, V. Yashchuk, and A. Weis, "Resonant nonlinear magneto-optical effects in atoms," *Reviews of modern physics* **74**, 1153 (2002).
 - ²⁸J. Qiu and K. Hirao, "The faraday effect in diamagnetic glasses," *Journal of materials research* **13**, 1358–1362 (1998).
 - ²⁹H. Takebe, S. Pujino, and K. Morinaga, "Refractive-index dispersion of tellurite glasses in the region from 0.40 to 1.71 μm ," *Journal of the American Ceramic Society* **77**, 2455–2457 (1994).
 - ³⁰D. Vojna, O. Slezák, A. Lucianetti, and T. Mocek, "Verdet constant of magneto-active materials developed for high-power faraday devices," *Applied Sciences* **9**, 3160 (2019).
 - ³¹P. Brint, E. Meshulam, and A. Gedanken, "Excited electronic states of limonene: A circular dichroism and photoelectron spectroscopy study of d-limonene," *Chemical physics letters* **109**, 383–387 (1984).
 - ³²M. Fujiki, Y. Kawagoe, Y. Nakano, and A. Nakao, "Mirror-symmetry-breaking in poly [(9, 9-di-n-octylfluorenyl-2, 7-diyl)-alt-biphenyl](pf8p2) is susceptible to terpene chirality, achiral solvents, and mechanical stirring," *Molecules* **18**, 7035–7057 (2013).
 - ³³K. Raghavachari, G. W. Trucks, J. A. Pople, and M. Head-Gordon, "A fifth-order perturbation comparison of electron correlation theories," *Chemical Physics Letters* **157**, 479–483 (1989).
 - ³⁴C. Hättig, D. P. Tew, and A. Köhn, "Communications: Accurate and efficient approximations to explicitly correlated coupled-cluster singles and doubles, ccsd-f12," *Journal of Chemical Physics* **132**, 231102 (2010).
 - ³⁵Y. J. Franzke, C. Holzer, J. H. Andersen, T. Begušić, F. Bruder, S. Coriani, F. Della Sala, E. Fabiano, D. A. Fedotov, S. Fürst, S. Gillhuber, R. Grotjahn, M. Kaupp, M. Kehry, M. Krstić, F. Mack, S. Majumdar, B. D. Nguyen, S. M. Parker, F. Pauly, A. Pausch, E. Perlt, G. S. Phun, A. Rajabi, D. Rappoport, B. Samal, T. Schrader, M. Sharma, E. Tapavicza, R. S. Treß, V. Voora, A. Wodyński, J. M. Yu, B. Zerulla, F. Furche, C. Hättig, M. Sierka, D. P. Tew, and F. Weigend, "Turbomole: Today and tomorrow," *Journal of Computational and Theoretical Chemistry* **10**, 1021/acs.jctc.3c00347.
 - ³⁶T. H. Dunning, "Gaussian basis sets for use in correlated molecular calculations. i. the atoms boron through neon and hydrogen," *Journal of Chemical Physics* **90**, 1007–1023 (1989).
 - ³⁷A. D. Becke, "A new mixing of Hartree-Fock and local density-functional theories," *The Journal of Chemical Physics* **98**, 1372–1377 (1993), https://pubs.aip.org/aip/jcp/article-pdf/98/2/1372/11046762/1372_1_online.pdf.
 - ³⁸P. J. Stephens, F. J. Devlin, C. F. Chabalowski, and M. J. Frisch, "Ab initio calculation of vibrational absorption and circular dichroism spectra using density functional force fields," *The Journal of Physical Chemistry* **98**, 11623–11627 (1994).
 - ³⁹F. Weigend and R. Ahlrichs, "Balanced basis sets of split valence, triple zeta valence and quadruple zeta valence quality for h to rn: Design and assessment of accuracy," *Physical Chemistry Chemical Physics* **7**, 3297–3305 (2005).
 - ⁴⁰F. Furche and D. Rappoport, "Tii - density functional methods for excited states: Equilibrium structure and electronic spectra," in *Computational Photochemistry*, Theoretical and Computational Chemistry, Vol. 16, edited by M. Olivucci (Elsevier, 2005) pp. 93–128.
 - ⁴¹T. Yanai, D. P. Tew, and N. C. Handy, "A new hybrid exchange–correlation functional using the coulomb-attenuating method (cam-b3lyp)," *Chemical Physics Letters* **393**, 51–57 (2004).
 - ⁴²D. Vala, M. Mičica, D. Cvejn, and K. Postava, "Broadband mueller ellipsometer as an all-in-one tool for spectral and temporal analysis of mutarotation kinetics," *RSC advances* **13**, 6582–6592 (2023).
 - ⁴³J. P. Greenstein, M. Winitz, *et al.*, *Chemistry of the amino acids* (Wiley, 1961).
 - ⁴⁴K. Hayashi, Y. Fujii, R. Saito, H. Kanao, and T. Hino, "The influence of measurement parameters on the specific rotation of amino acids: Part I. The Effect of Solute and Hydrochloric Acid Concentration on Optical Rotation, Part II. The Effect of Sulfuric Acid Concentration to Specific Rotation," *Agricultural and Biological Chemistry* **30**, 1221–1237 (1966).
 - ⁴⁵S. Rossi, P. Lo Nostro, M. Lagi, B. W. Ninham, and P. Baglioni, "Specific anion effects on the optical rotation of α -amino acids," *The Journal of Physical Chemistry B* **111**, 10510–10519 (2007).
 - ⁴⁶*Organic Chemistry*, 9th ed. (McGraw-Hill Education, 2013).
 - ⁴⁷M. D. Kundrat and J. Autschbach, "Computational modeling of the optical rotation of amino acids: A new look at an old rule for pH dependence of optical rotation," *Journal of the American Chemical Society* **130**, 4404–4414 (2008).